34th Annual International Conference of the IEEE EMBS
San Diego, California USA, 28 August - 1 September, 2012

A Personalized Mitral Valve Closure Simulator

P. Burlina[1,2], R. Mukherjee[1], C. Sprouse [1]

Abstract— **We describe a method for performing modeling and simulation to predict the closure of the Mitral Valve (MV) using patient specific anatomical information derived from 3D Transesophageal Echocardiography (3D TEE). The ability to predict the MV closure behavior is an important step along the way of developing personalized simulation tools that would allow a surgeon to perform preoperative planning and decide between various MV repair options. While the MV is an important use case because of its relevance and prevalence among reconstructive cardiac interventions, the study described here can provide a blueprint to perform pre-operative planning for other cardiac surgical interventions. The method reported here exploits the Saint Venant-Kirchhoff elasticity model that is tuned to match empirical observations of the MV strain-stress behavior. Using intraoperative 3D TEE data, the proposed simulator was evaluated over 10 test cases and resulted in mean prediction absolute error values of 1.81 mm.**

I. Introduction

Our study is motivated by challenges faced by surgeons in carrying out reconstructive cardiac surgical interventions, which are performed on a flaccid heart. Among all cardiovascular diseases, the test case considered here is mitral valve disease (MVD) because of its clinical relevance and the surgical prevalence of MV reconstruction (valvuloplasty). Valvuloplasty is performed on an arrested heart under cardiopulmonary bypass. It is therefore difficult for the surgeon to predict how the modified valve will perform once the heart is restarted and the MV is immersed in physiological conditions. Planning via simulation would allow a surgeon to evaluate the risks and benefits associated with a specific surgical option. Such systems would allow the surgeon to evaluate the quality of the reconstructive procedure by inspecting the resulting predicted postoperative anatomy and physiology (as was done in [1], [2]). This would be an important tool considering the increased postoperative mortality and morbidity associated with procedures performed in hospitals with lesser operative volumes [3].

The MV is a key anatomical structure with a critical function, to ensure unidirectional flow of blood from left atrium (LA) to left ventricle (LV). It is located in the left heart complex, and consists of an annulus with two leaflets tethered through a complex system of chords (termed *chordae tendineae*) attached to a set of papillary muscles. A measure of quality of repair uses the degree of contact (coaptation) between these leaflets when the valve closes. The goal of our study is to predict valve closure based on an assumed open valve configuration. The planning process starts with an open 3D valve structure at diastole, derived by segmenting Real Time 3D Echocardiography (RT3DE) imagery and edited by a surgeon to remove artifacts and reflect the planned surgical modifications. From the open valve, our system predicts, via physics-based modeling and simulation, the closed valve configuration at systole to characterize the MV leaflets' ability to competently coapt.

Much progress has been made in MV mechanical modeling ([1], [2], [4], [5], [6], [7], [8], [9], [10], [11]). Recent efforts have focussed on exploiting patient specific information for surgical planning and guidance. In particular, Real time 3D TEE has enabled cardiac simulation using patient-specific anatomy, and also notably, the evaluation of predictive models against ground truth (e.g. [1], [2], [12], [13], [14], [15]).

This paper extends our work reported in [2] and presents a number of additional enhancements in the prediction model and the validation methods, including: we now use (a) physiological blood loading forces (with direction along the leaflet surface normals and with physiological pressure), (b) elastic forces based on the Saint Venant-Kirchhoff model tuned to approximate the empirical MV leaflets' strain-stress behavior found by May-Newman in [16], (c) physiological values for all other entities, and (d) both marginal and basal chordae for modeling; we use (e) patient-specific chordal lengths, (f) personalized annulus shapes, and (g) patient-specific annulus deformations between open and closed configurations. In this paper we also also tie the MV stationary shape finding technique to first principles by using Lagrangian mechanics, to demonstrate that it is a well principled mechanical modeling approach. These various enhancements have significantly lowered the prediction error from about 4-5mm in [2] to presently an average of 1.81mm.

II. Methods

Our process is initiated by segmenting the left heart endocardial and valvular structure from 3D TEE using a thin tissue detection approach reported in [17]. The segmentation is vetted and corrected by an expert. A mesh is fitted to the segmented leaflets and lower atrium. The mesh describes the state of the valve system in the open position. Each node of the mesh introduces three degrees of freedom to the problem of finding the final closed configuration. Each node has an associated energy term resulting from external forces (consisting of blood pressure), internal strain energy, collision energy preventing intersection with other portions of the mesh, and tethering energy created by the chordae tendineae. The total energy of the system is then minimized so as to find the displacement taking the mesh from its open

[1]The Johns Hopkins University Applied Physics Laboratory, Laurel, MD 20723 [2]The Johns Hopkins University Department of Computer Science, Baltimore, MD 21218

configuration to a stationary configuration point representing the mesh at closed position. Details are now presented.

We start by modeling the mitral valve system in the context of Lagrangian mechanics to tie the stationary method to first principles. The Lagrangian of the system is expressed as

$$L = \phi_{kin} - \phi_{pot} \tag{1}$$

where the kinetic energy ϕ_{kin} from each MV mesh node i is

$$\phi_{kin} = \sum_i \frac{1}{2} M_i \dot{q_i}^2 \tag{2}$$

The variables q_i denote the degrees of freedom of the system, i.e. the x, y, z coordinates for the position of each node in the valve mesh, and the terms $\dot{q_i}$ are their time derivatives. M_i are the masses associated with each element. The potential energy is given by

$$\phi_{pot} = \sum_i \phi_i^X + \phi_i^E + \phi_i^T + \phi_i^C \tag{3}$$

where ϕ_i^X is the external energy, ϕ_i^E is the strain energy, ϕ_i^T is the tethering energy, and ϕ_i^C is the collision energy. The expressions for these terms are detailed later. Lagrange's equations are given by

$$\frac{d\left(\frac{\partial L}{\partial \dot{q_i}}\right)}{dt} - \frac{\partial L}{\partial q_i} = -\frac{\partial F_i^{diss}}{\partial \dot{q_i}} \tag{4}$$

where F_i^{diss} is the Rayleigh dissipation function for each component i, defined by

$$F_i^{diss} = \frac{1}{2} C \dot{q_i}^2 \tag{5}$$

An expression directly involving the dissipative force is obtained by considering that

$$F_i \equiv -\frac{\partial F_i^{diss}}{\partial \dot{q}} = -C\dot{q_i} \tag{6}$$

so that Lagrange's equations become

$$\frac{d\left(\frac{\partial L}{\partial \dot{q_i}}\right)}{dt} - \frac{\partial L}{\partial q_i} = F_i \tag{7}$$

The previous equation would be the basis for seeking the closure using a dynamic method taking the valve configuration from late diastole to systole. For our system, the potential energy depends only on q_i since we have conservative forces. Then the first term in Lagrange's equations only involves the kinetic energy and becomes

$$\frac{d\left(\frac{\partial L}{\partial \dot{q_i}}\right)}{dt} = M\ddot{q_i} \tag{8}$$

so that finally

$$M\ddot{q_i} - \frac{\partial L}{\partial q_i} = F_i \tag{9}$$

Considering the system at the stationary position (i.e. at rest, where $\dot{q} = \ddot{q} = 0$), Lagrange's equations yield a necessary condition on the gradient of the Lagrangian of the stationary system

$$\frac{\partial L}{\partial q_i} = 0 \tag{10}$$

or alternatively:

$$\nabla_{\mathbf{q}} L = 0 \tag{11}$$

The stationary configuration is therefore found as the solution for the problem

$$\mathbf{q}^* = argmin_{\mathbf{q}}(\phi_{pot}) \tag{12}$$

The initial state configuration of the open mesh is used to specify the zero energy point for external (fluid pressure), elastic (strain), and tethering forces. The zero energy point for the collision force preventing mesh intersections is the configuration in which all facets of the mesh are not contacting (more specifically, further apart than a threshold distance δ). The closed state is found as the stationary point determined by solving the above energy minimization problem. The specification of the different additive components for the energy in $\phi_i = \phi_i^X + \phi_i^E + \phi_i^T + \phi_i^C$ are now detailed.

a) Blood loading energy: Blood loading energy is modeled as

$$\phi_i^X = -p_0 \mathbf{n}_i \cdot \mathbf{d}_i \tag{13}$$

where $\mathbf{n_i}$ is the surface normal at node i, p_0 is the blood pressure, and $\mathbf{d}_i$ is the displacement vector of node i.

For each facet on the valve leaflets, the direction of the blood pressure forces is specified to lie along the facet normal pointing toward the atrium. The pressure is set to be 13.3 kPa (or 100 mm Hg).

b) Strain energy: The leaflets are modeled as membranes. We denote the second Piola-Kirchhoff stress at each facet j by $\mathbf{S}_j$ and the Lagrangian Green strain at each facet by $\mathbf{E}_j$.

The strain energy for each node i is given by

$$\phi_i^E = \frac{1}{2} \sum_{j \in \Lambda_i} \frac{A_j d}{3} \boldsymbol{S}_j \cdot \boldsymbol{E}_j \tag{14}$$

where, for each i, the sum is taken over the set Λ_i of all adjacent facets j containing the node i, A_j denotes the area of the undeformed facet j, and d denotes the membrane thickness. For plane stress, we vectorize the stress and strain tensors as $\boldsymbol{E} = (E_{xx}, E_{yy}, \sqrt{2}E_{xy})^T$ and $\boldsymbol{S}_j = (S_{xx}, S_{yy}, \sqrt{2}S_{xy})^T$. Our stress-strain relationship uses the Saint Venant-Kirchhoff model

$$\boldsymbol{S}_j = \mathbf{H}\boldsymbol{E}_j \tag{15}$$

where the elasticity matrix $\mathbf{H}$ of the mesh can be written in terms of the Young modulus of elasticity, E, and the Poisson ratio, ν, as

$$\mathbf{H} = \frac{E}{1-\nu^2} \begin{pmatrix} 1 & \nu & 0 \\ \nu & 1 & 0 \\ 0 & 0 & 1-\nu \end{pmatrix} \tag{16}$$

The numerical values taken for our system are set as follows: the Poisson ratio for the anterior and the posterior leaflets is taken to be $\nu = 0.5$, which is the value for an incompressible material; the Young modulus is set to $E = 100$ kPa for the posterior leaflet and $E = 400$ kPa for the anterior leaflet, to reflect the fact that the posterior leaflet is more pliable than the anterior leaflet, and so as to generate strains and stresses that are consistent with strain-stress MV leaflets behavior determined empirically by May-Newman (see [16]). The leaflet thickness is taken to be 1 mm. The resulting behavior of the stretch-stress function in the frame of reference of the deformed facets (using Cauchy stress) is plotted for different stretch situations and for the anterior and posterior leaflets in Fig. 1 for the strip biaxial stretching case. This plot exemplifies the stretch-strain behavior and as can be noted, the strain-stress relationship in the deformed frame of reference is nearly (but not exactly) linear.

Tethering and collision energy are not detailed here since they identical to those used in our prior study in [2].

c) Annulus deformation: To account for changes in annulus shape between diastole and systole in a way that is patient-specific, an expert first segments both the open and closed state annuli from 3D TEE imagery. Expert annulus segmentations are then converted to NURBS curves, which are used to generate an approximate scaling value that is representative of how much the annulus contracted or expanded between late diastole and begin systole. The entire open state mesh is then deformed according to this scaling value, keeping the undeformed state as the simulation energy reference point for computing strain and stress (i.e. the accrued energy due to the leaflet's stretching resulting from the annulus deformation is taken into account to seek the stationary closed MV configuration).

d) Chordal length estimation: Finally, we estimate the chordal lengths, which can not be easily assessed from 3D TEE imagery in a way that best represents the patient. To accomplish this, we run our simulation by varying the chordal lengths about a nominal set of lengths multiplied by a scaling factor. This nominal set of lengths are computed by first considering the distance from the papillary muscles positions to the chordal attachments, which then represent a set of assumed and approximate late diastole chordal lengths (EDCL). The estimated lengths are then found by seeking the scaling factor that best represents the patient, in a way that minimizes the prediction error, i.e. the error between the valve closure configuration predicted by our system, and the actual closed configuration derived by segmentation at systole. More details are provided in the experimental methods section.

III. Results

We now describe our modeling validation framework: it consists of using real 3D TEE patient data and computing errors by comparing predicted and actual closed configurations.

Data acquisition and cases studied: We collected intra-operative real-time 3D TEE full-volume data sequences of mitral valves from patients of the Johns Hopkins University's School of Medicine. TEE sequences were acquired under a protocol approved by the JHU Institutional Review Board from patients who gave informed consent. Most of these patients underwent Coronary Artery Bypass Grafting (CABG), and were mostly asymptomatic with regard to mitral valve disease, except for patient number one. TEE acquisition was performed using an iE33 Philips console with an X7-2t probe (Philips Medical Systems, Bothell, WA). Of all the sequences acquired, only a subset were usable in this study (sequences entailing cropped MVs, severe stitching artifacts, or insufficient resolutions were eliminated). This resulted in a testing dataset of nine separate sequences corresponding to six different patients. Two of the cases entailed predicting closure from two different open positions in the same sequence (test cases 3 and 4), resulting in 10 test cases in all being performed. The TEE cube sizes were $224 \times 208 \times 208$ voxels, measured along the elevational, lateral, and axial directions[1]. The 4D TEE probe was run at frequencies ranging from 3 to 5 MHz[2]. The spatial resolutions ranged from approximately 0.4 to 0.8 mm. The data was collected intraoperatively using a seven breath-hold cycle protocol leading to maximal frame rates close to 50 Hz.

Testing and results: Frames in the sequence corresponding to late diastole and systole were automatically segmented. The chordal lengths, specific to each patient, were found via optimization by seeking the length scaling factor that best describes the patient, i.e. minimizes the prediction error. In our models, the chords included both marginal (also called primary) and basal (also called secondary) chordae tendineae. Marginal chords prevent the leaflet edges from moving into the LA, basal chords' retentive action prevents prolapsing of the mitral leaflets. In average, a total of three basal chords and four marginal chords per leaflet were placed manually for each case, by looking for cues of chordal insertions from the TEE data and resulting meshes, or when this was unavailable, by distributing them based on prior anatomical knowledge. This resulted in a total of about fourteen chords per MV. Two papillary muscle heads were manually specified for each case. As explained in the previous section, the annuli in open and closed configurations were hand segmented from the 3D TEE frusta, and a dilation

[1]These are the canonical directions for 3D echography: i.e., the axial direction is along the acoustic path and corresponds to the z-axis, and the lateral-elevational plane corresponds to the x-y plane parallel to the plane containing the echographic transducers.

[2]The iE33 platform does not allow fine selection of the transmit frequency. Instead, the user adjusts the frequency by selecting one of three settings (Penetration, General, and Resolution) that can be set using the "2D Opt" control. Additionally, the actual frequency is not recorded in the DICOM headers, therefore only a range of frequencies can be reported here. 3-7 MHz are possible in this platform.

(or contraction) factor was computed from open to closed position and was applied on the open mesh annulus prior to running the simulation so as to reflect a transformation to the closed mesh annulus.

For those inputs that required manual intervention (chordal attachments, papillary head placement, valve annulus), no attempt was made in this study at exhaustively evaluating positioning so as to get the best error performance; instead, these were set once and the chordal length optimizations/simulations were then run. Similarly, all the mechanical model parameters described in the previous section were set once and for all, and remained the same across each case (their value was detailed in the previous section).

Figure 3 shows close ups of the initial and final computed configurations for one of the test cases. Color coded areas correspond to the anterior (red) and posterior (blue) leaflets. Note that the red and blue areas include parts of the attached primary chordae tendineae structure. The yellow area includes the annulus as well as the lower part of the atrium.

The quantitative evaluation involved measuring the errors between predicted and ground truth, and are summarized in Table I. We also show the error map distribution for one of the cases in Figure 2. We compared the predicted closed valve mesh with the actual segmented closed valve mesh, by first registering the two meshes, as was done in [13], to adjust for the mostly vertical translation of the annulus during closure. The simulated mesh was then cropped to include only what would be "visible" to the ultrasound probe. This visibility cropping matches how the ground-truth segmentation is obtained (only a thin layer of tissue nearest the ultrasound probe is segmented), and prevents the computation of error in obstructed areas below the valve for which ground truth is difficult to obtain due to shadowing and noise. Finally, the error is calculated as the average of minimum distances between the centroids of facets on the simulated mesh to the centroids of facets on the ground truth. The results reported also correspond to the optimal tether length estimation (labeled "(OPT)") and include, for comparison, the mean error found for the late diastole chordal length of the tether without any further optimization (labeled "(EDCL)").

From Table I, the mean absolute errors appear to be on the order of the 3D TEE spatial resolution. The magnitudes of errors we find are, in absolute terms, comparable to the results reported in a recent paper by [14], who also used 3D TEE, but different finite element model and valve tracking approaches, but where errors are measured in a different fashion (simulated to tracked position discrepancy). The magnitudes of the errors found in this study are also comparable, when considering the spatial resolution limitations of the imaging modalities used (i.e. when measured in voxels), with the results reported in [13], who relied on micro-CT with resolution of about 100 μm and with a modeling method based on linear or piecewise-linear mass-spring models. Such comparisons however should be considered with caution, as there are differences between the different imaging modalities, datasets, and methods used in these studies that make it difficult to directly compare error results.

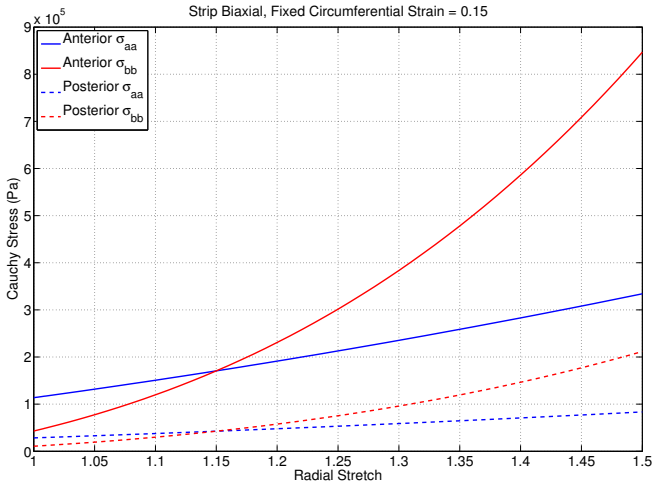

Fig. 1. Stress-strech relationship for our Saint Venant-Kirchhoff elasticity model tuned to approximate the MV behavior found empirically by May-Newman in [16]. Strip biaxial stretching case (circumferential is pre-streteched at 15% and and radial stretches are applied). Laws are shown for both anterior and posterior leaflets.

TABLE I

PREDICTION ERROR STATISTICS.

Case	Patient	(OPT) Mean	Std	5%	95%	(EDCL) Mean
1	1	1.81	1.32	0.25	4.29	1.93
2	2	2.25	1.38	0.37	4.54	2.25
3	2	2.41	2.56	0.22	7.38	3.30
4	2	2.01	1.98	0.21	6.26	2.31
5	3	1.39	0.97	0.19	3.21	1.76
6	4	1.69	1.47	0.20	4.78	1.96
7	5	1.33	1.19	0.19	3.56	2.28
8	6	2.53	2.13	0.25	6.62	2.98
9	3	1.46	1.33	0.18	4.00	1.46
10	1	1.86	1.53	0.23	5.28	1.90
all	all	1.86	1.72	0.21	5.27	2.21

error map

IV. CONCLUSION

We presented a new RT3DE-guided physics-based modeling and simulation procedure based on Saint Venant-Kirchhoff tissue modeling and using a static load analysis and optimization and using realistic physiological forces. Testing with clinical data shows promising results with regard to prediction error. Future work will incorporate patient-specific dynamic information as obtained in [18], [19] for modeling purposes.

ACKNOWLEDGMENTS

This project was supported in part by JHU APL Science and Technology Research and Development funds and by NIH NHLBI R21HL098765. The content is solely the responsibility of the authors and does not necessarily represent the official views of the National Heart, Lung, And Blood Institute or the National Institutes of Health.

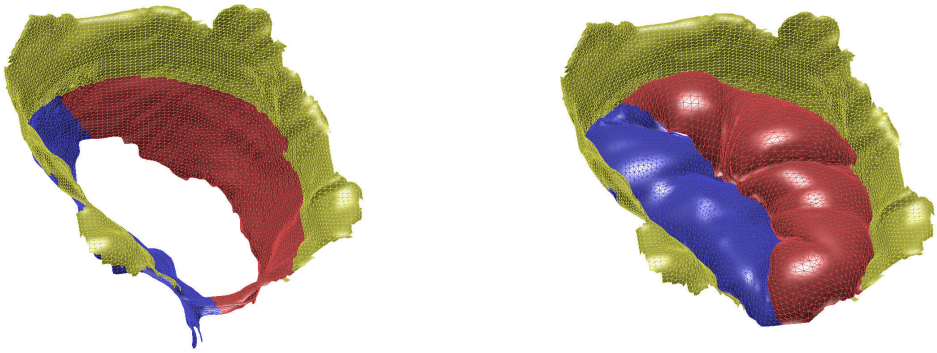

Fig. 3. Initial open valve configuration from TEE segmentation and closed configuration predicted using mechanical modeling (case 1).

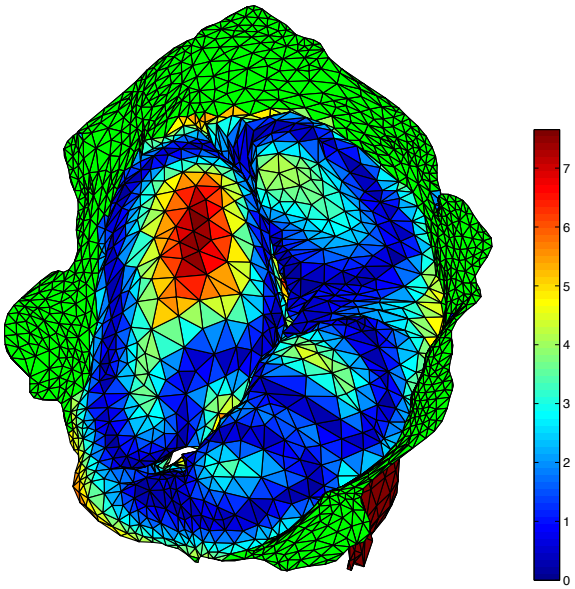

Fig. 2. Error map is shown and shows the variation of the error distribution for various parts of the valve (case 1).

REFERENCES

[1] C. Sprouse, D. Yuh, T. Abraham, and P. Burlina, "Computational hemodynamic modeling based on transesophageal echocardiographic imaging," *Proc. Int. Conf. Engineering in Medicine and Biology Society*, vol. 2009, pp. 3649–3652, 2009.

[2] P. Burlina, C. Sprouse, D. DeMenthon, A. Jorstad, R. Juang, F. Contijoch, T. Abraham, D. Yuh, and E. McVeigh, "Patient-specific modeling and analysis of the mitral valve using 3D-TEE," *Information Processing in Computer-Assisted Interventions*, pp. 135–146, 2010.

[3] J. Gammie, S. O'Brien, B. Griffith, T. Ferguson, and E. Peterson, "Influence of hospital procedural volume on care process and mortality for patients undergoing elective surgery for mitral regurgitation," *Circulation*, vol. 115, no. 7, p. 881, 2007.

[4] M. Sacks, Y. Enomoto, J. Graybill, W. Merryman, A. Zeeshan, A. Yoganathan, R. Levy, R. Gorman, and J. Gorman, "In-Vivo Dynamic Deformation of the Mitral Valve Anterior Leaflet," *The Annals of Thoracic Surgery*, vol. 82, pp. 1369–1377, 2006.

[5] V. Prot, B. Skallerud, and G. Holzapfel, "Transversely isotropic membrane shells with application to mitral valve mechanics. Constitutive modelling and finite element implementation," *Int. Journal for Numerical Methods in Engineering*, vol. 71, no. 8, pp. 987–1008, 2007.

[6] D. Einstein, F. Del Pin, X. Jiao, A. Kuprat, J. Carson, K. Kunzelman, R. Cochran, J. Guccione, and M. Ratcliffe, "Fluid-structure interactions of the mitral valve and left heart: Comprehensive strategies, past, present and future," *Int. Journal for Numerical Methods in Biomedical Engineering*, vol. 26, no. 3-4, pp. 348–380, 2010.

[7] E. Votta, E. Caiani, F. Veronesi, M. Soncini, F. Montevecchi, and A. Redaelli, "Mitral valve finite-element modelling from ultrasound data: a pilot study for a new approach to understand mitral function and clinical scenarios," *Philosophical Transactions of the Royal Society A: Mathematical, Physical and Engineering Sciences*, vol. 366, no. 1879, p. 3411, 2008.

[8] K. Kunzelman, R. Cochran, C. Chuong, W. Ring, E. Verrier, and R. Eberhart, "Finite element analysis of the mitral valve." *The Journal of Heart Valve Disease*, vol. 2, no. 3, p. 326, 1993.

[9] D. Einstein, K. Kunzelman, P. Reinhall, M. Nicosia, and R. Cochran, "Non-linear fluid-coupled computational model of the mitral valve." *The Journal of Heart Valve Disease*, vol. 14, no. 3, p. 376, 2005.

[10] K. Lau, V. Diaz, P. Scambler, and G. Burriesci, "Mitral valve dynamics in structural and fluid-structure interaction models," *Medical engineering & physics*, vol. 32, no. 9, pp. 1057–1064, 2010.

[11] P. Watton, X. Luo, X. Wang, G. Bernacca, P. Molloy, and D. Wheatley, "Dynamic modelling of prosthetic chorded mitral valves using the immersed boundary method," *Journal of Biomechanics*, vol. 40, no. 3, pp. 613–626, 2007.

[12] P. E. Hammer, D. P. Perrin, P. J. del Nido, and R. D. Howe, "Image-based mass-spring model of mitral valve closure for surgical planning," in *Proc. of SPIE*, San Diego, CA, USA, 2008, pp. 69 180Q–69 180Q–8.

[13] P. Hammer, P. del Nido, and R. Howe, "Anisotropic mass-spring method accurately simulates mitral valve closure from image-based models," *Functional Imaging and Modeling of the Heart*, pp. 233–240, 2011.

[14] T. Mansi, I. Voigt, E. Mengue, R. Ionasec, B. Georgescu, T. Noack, J. Seeburger, and D. Comaniciu, "Towards patient-specific finite-element simulation of mitralclip procedure," *Medical Image Computing and Computer-Assisted Intervention–MICCAI 2011*, pp. 452–459, 2011.

[15] M. Stevanella, G. Krishnamurthy, E. Votta, J. Swanson, A. Redaelli, and N. Ingels Jr, "Mitral leaflet modeling: Importance of in vivo shape and material properties," *Journal of biomechanics*, 2011.

[16] K. May-Newman and F. Yin, "A constitutive law for mitral valve tissue," *Journal of Biomechanical Engineering*, vol. 120, p. 38, 1998.

[17] P. Burlina, R. Mukherjee, R. Juang, and C. Sprouse, "Recovering endocardial walls from 3D TEE," *Functional Imaging and Modeling of the Heart*, pp. 284–293, 2011.

[18] P. Burlina, B. Hoffmann, and T. Abraham, "Computing left ventricular hemodynamics from echographic optical flow of CEUS microspheres," in *IEEE/NIH Life Science Systems and Applications Workshop*, 2011, pp. 67–72.

[19] R. Mukherjee, C. Sprouse, A. Pinhero, T. Abraham, and P. Burlina, "Computing myocardial motion in 4D TEE," *Ultrasound in Medicine and Biology (in press)*, 2012.